Navigation Between Geosynchronous and Lunar L1 Orbiters

Jeffrey S. Parker* and Rodney L. Anderson†

Jet Propulsion Laboratory, California Institute of Technology, Pasadena, CA 91109, USA

George H. Born‡, Kohei Fujimoto§, Jason M. Leonard§, and Ryan M. McGranaghan§

University of Colorado, Boulder, CO 80309, USA

Linked Autonomous Interplanetary Satellite Orbit Navigation (LiAISON) is a new technique that takes advantage of the asymmetrical gravity field present in a three-body system in order to perform *absolute* tracking of satellites using only relative satellite-to-satellite observations. Previous studies have demonstrated LiAISON's practical applications for lunar missions, including a satellite in a halo orbit about either the Earth-Moon L_1 or L_2 point. This paper studies the viability of applying LiAISON measurements between a lunar halo orbiter and a satellite in a geosynchronous orbit. Simulations demonstrate that the absolute positions and velocities of both satellites are observable using only relative measurements with an achieved uncertainty on the order of observation noise.

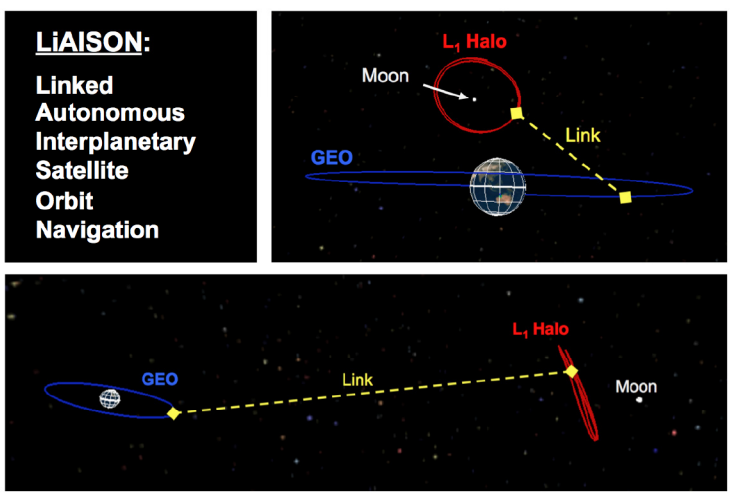

Figure 1. The constellation studied in this paper includes a satellite in geosynchronous orbit and a satellite in a halo orbit about the Earth-Moon L_1 point tracking each other. The plots are visualized in the Earth-Moon rotating coordinate frame.

*Member of Technical Staff, Jet Propulsion Laboratory, California Institute of Technology, M/S 301-121, 4800 Oak Grove Dr., Pasadena, CA 91109, AIAA Senior Member. Currently an Assistant Research Professor at the University of Colorado, Boulder, CO 80309.

†Member of Technical Staff, Jet Propulsion Laboratory, California Institute of Technology, M/S 301-121, 4800 Oak Grove Dr., Pasadena, CA 91109, AIAA Member.

‡Director of the Colorado Center for Astrodynamics Research, University of Colorado, Boulder, CO 80309, AIAA Fellow.

§Research Assistant, University of Colorado, Boulder, CO 80309, AIAA Student Member.

I. Introduction

RECENT advances have revealed new ways to use relative satellite-to-satellite tracking (SST) data to perform absolute navigation of one or more satellites. The Global Positioning System (GPS) has revolutionized satellite navigation in low Earth orbit using SST measurements. A new technique called LiAISON (Linked Autonomous Interplanetary Satellite Orbit Navigation) propels the successful aspects of GPS to new orbits, including geosynchronous orbits, lunar orbits, and lunar libration orbits. Where GPS requires ground tracking to anchor the entire constellation to the surface of the Earth, LiAISON may be used independently of ground stations. Further, LiAISON requires as few as two cooperative satellites to be successful.

Previous research efforts have demonstrated LiAISON applied to lunar constellations, where satellites are placed in lunar libration orbits, such as halo orbits, and/or in low lunar orbits.[1–8] It has been shown that a constellation of only two satellites, where one is in a libration orbit and one is in a low lunar orbit, can use scalar SST measurements, such as range or range-rate, and successfully determine both their relative and absolute positions and velocities in space over time.[3] High-fidelity simulations have demonstrated autonomous navigation that yield error uncertainties within 10 meters in position for the low lunar orbiter and 100 meters in position for the halo orbiter without any ground-based tracking. Such simulations include realistic schedules of measurements, permitting both satellites to perform other non-compatible tasks.

A dedicated navigation satellite in a lunar libration orbit may be employed to support numerous lunar satellites. It is postulated that such a navigation satellite may also have periods of time when its services are not required at the Moon. While the communication link distance is far greater, the navigation satellite at the Moon may also be used to improve the navigation support of satellites in orbit about the Earth.

The research presented in this paper explores the application of LiAISON navigation to a new system of two satellites, where one is in a lunar libration orbit about the Earth-Moon L_1 (LL_1) and the other is in a geosynchronous (GEO) orbit, as illustrated in Figure 1. Conventional satellite navigation in GEO is plagued by the relatively small amount of change observed over time between the satellite and any ground station. This paper shows that LiAISON navigation not only works in this system, but offers improved navigation accuracy for a GEO satellite, especially when compared with radiometric tracking data. A simplified simulation of LiAISON navigation achieves absolute position uncertainties below 1 meter for both the libration orbiter and the GEO satellite even without any ground tracking. Further efforts are required to study the benefits of LiAISON in a high-fidelity realistic scenario,[9] but the work presented here demonstrates that the concept is successful and potentially very valuable to the satellite navigation community.

II. Background

A. Lunar LiAISON

The concept of LiAISON was first formulated in 2005 by Hill et al.[1,2] Hill et al. noticed that a time-series of scalar satellite-to-satellite tracking observations contains more information in an asymmetric force field than they do in a symmetric force field.[1] Indeed, it is well known that the time-series of relative observations between multiple Earth orbiting satellites appears identical if the entire constellation of Earth orbiters is rotated about the Earth, provided that the observations are not sensitive enough to notice anything more subtle than the Earth's point-mass gravitational field. In that case, only a subset of the constellation's orbital parameters may be determined using relative measurements, such as the semi-major axis of each satellite's orbits.[10] Solar radiation pressure and the Earth's J_2 effect (or higher-order gravity terms, if the measurements are sensitive enough) are two sources of asymmetry that may reveal more information about the absolute locations of each satellite. The most dramatic asymmetries in the force field originate near the Moon, where the lunar gravity significantly influences a satellite's acceleration over time. Unique SST signatures are easily available if one of the satellites is significantly influenced by the Moon. Of course the observational problem returns if all satellites are deep within the Moon's gravity field, where the Earth's gravity becomes a minor perturbation.

In the simplest case, one considers two satellites and their mutual SST observations. The SST observations contain the most information if one satellite is bound to the Earth and one is bound to the Moon. A libration orbit about LL_1 or LL_2 is tied to both the Earth and the Moon. Hence, if one satellite is traversing such a libration orbit, the other satellite may be located at the Earth or the Moon or even in another libration orbit and the formation generates unique SST signatures. Hill et al. demonstrated that the full state space of both satellites is observable for the case that one is in a libration orbit about LL_1 or LL_2 and the other

is in a low lunar orbit.[2] Hill extended the concept to study constellations of 2–4 satellites in a wide variety of architectures at the Moon, provided that at least one of the satellites is in a libration orbit about LL_1 or LL_2.[6]

One particular case has been thoroughly studied, simulating a practical navigation mission at the Moon.[3,6] Two satellites are transferred together to an LL_2 orbit following a low-energy lunar transfer, where one satellite remains and the other is deployed and descends down to a 100 km polar low lunar orbit. The resulting architecture is illustrated in Figure 2. The simulation involves as many realistic components as possible, including high-fidelity dynamical models, realistic maneuver execution models, realistic observation schedules, etc. The two satellites track each other using relative range and range-rate observations, including measurement errors. The results indicate that the low lunar orbiter's state may be estimated to within 10 meters in position and 1 cm/s in velocity over time and the LL_2 halo orbiter's state may be estimated to within 100 meters in position and 1 mm/s in velocity over time (1σ). No ground observations were included in any lunar LiAISON simulation.

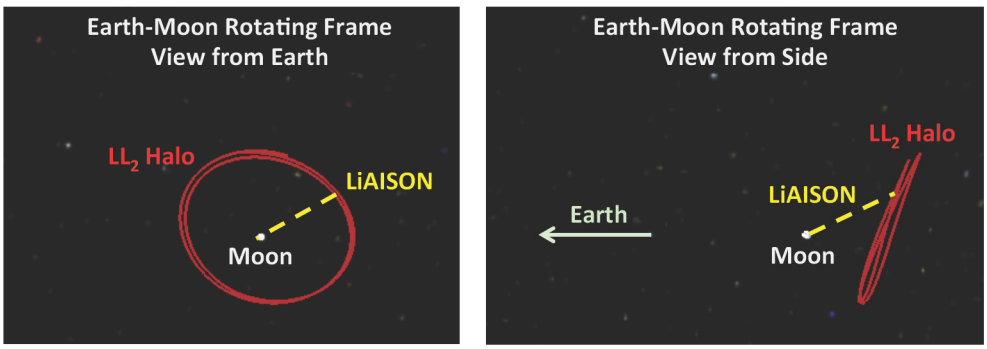

Figure 2. An illustration of LiAISON applied to the case of one satellite in a halo orbit about LL_2 and a satellite in a 100 km polar lunar orbit performing autonomous mutual navigation.

The results of previous work studying the lunar LiAISON problem demonstrate that a constellation of two or more satellites may be used to autonomously navigate any number of customers near the Moon. This is an interesting result because the system requires no ground observations at all. It is more likely that any practical near-future LiAISON observations that are made will supplement ground observations, reducing the work required by ground assets and/or improving the navigation accuracy, rather than replacing the ground observations entirely. As such, one may argue that a single navigation satellite may be optimized to provide a LiAISON beacon to other non-cooperative customers (i.e., customers that do not transmit tracking signals back to the navigation satellite), provided that ground observations accompany its observations. This reduces the total hardware required to achieve LiAISON at the Moon for practical purposes.

B. GEO Navigation

Most commercial geostationary satellites are tracked to within a kilometer in position. The TDRSS system has a requirement that it must be navigated to better than 100 meters in position, though in practice the solutions tend to be accurate to within 30 meters in position.[11] Sabol describes how range-only measurements may be used to determine GEO orbits to within 30 meters in position by combining measurements from several different ground stations.[12] Moreau et al. showed using simulations that one can use GPS signals from the far side of the Earth to improve this knowledge to about 15 meters.[13] Tombasco demonstrated that optical tracking may be used to reduce the three-dimensional uncertainty to within 10 meters.[14] With a proper receiver it is possible to use GPS signals and achieve position accuracies below 10 meters.[15] It is likely that supplementing ground tracking measurements with range or range-rate measurements between the GEO satellite and the Moon will only improve the solution, since the Moon provides an ever-changing geometry. It may be the case that LiAISON navigation improves the solution enough that only basic low-cost ground-based tracking is required at all.

C. Lunar Libration Navigation

The two ARTEMIS spacecraft were the first satellites to traverse trajectories about the LL_1 and LL_2 points, arriving in late 2010 and remaining in libration orbits through mid-2011 before descending to lower lunar orbits.[16,17] They did so using a significant amount of ground-based tracking from the Deep Space Network (DSN), the Universal Space Network (USN) and the Berkeley Ground Station (BGS) located at the University of California at Berkeley.[18,19] The navigation data included range and Doppler observations from DSN and USN antennae and Doppler observations from BGS. The nominal strategy involved collecting 3.5 hours of DSN tracking data every other day, alternating between stations in the northern and southern hemispheres, two 45-minute tracks of BGS data every day, and one 30-minute track of USN data per week.[19] Navigators were able to determine each of the satellites' states to within approximately 100 meters in position and approximately 1 mm/s in velocity at any time.[18] Each spacecraft performed station keeping maneuvers approximately once per week while in libration orbits, requiring approximately 0.5 m/s per month of ΔV.

D. LL_1–GEO LiAISON Navigation

It is straightforward to envision a scenario where a GEO satellite and a lunar libration orbiter are both being tracked by ground stations, such that the navigation solutions result in knowledge of both satellites' states within some uncertainty distribution. If one then introduces crosslink observations between the two satellites, the error distributions of each satellite will shrink in that relative direction, depending on the quality of the observations. Over time, this crosslink geometry will reduce the uncertainty in each dimension as the geometry of the system evolves. Figure 3 illustrates two of the interior angles in the time evolution of a triangle between the Earth, an example LL_1 orbiter, and an example GEO satellite to illustrate the strength of the geometry. The orbits will be described in more detail in Section III. For reference, the maximum angle between two ground stations as viewed by this LL_1 satellite is approximately 2.3°: far less than the 7–8 deg max angle illustrated in Figure 3. Similarly, the maximum angle between two ground stations as viewed by a GEO satellite is approximately 17.2°, not accounting for ground station horizon masks and operational constraints. Figure 3 illustrates that the crosslink angles have a much more dynamic range and should result in better state observation than ground-only measurements.

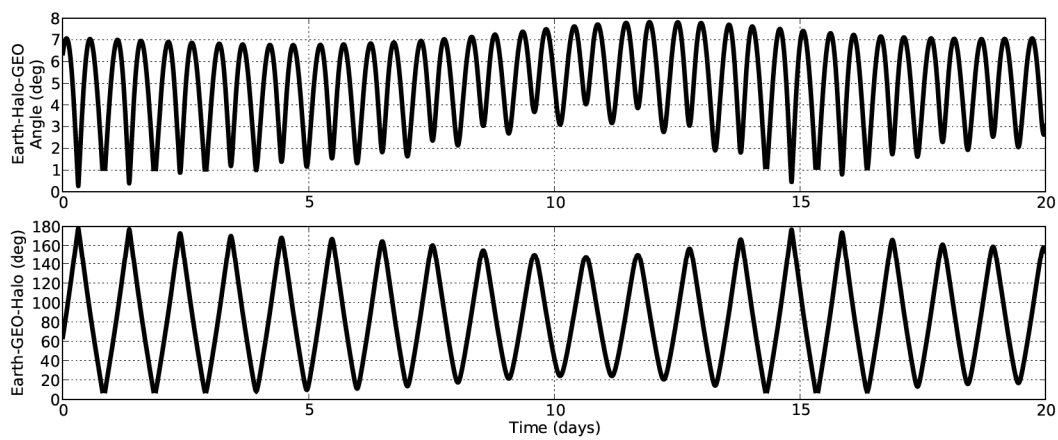

Figure 3. Two angles useful to evaluate the strength of tracking measurements between a GEO satellite and a libration orbiter about LL_1: the Earth-Halo-GEO angle (top) and the Earth-GEO-Halo angle (bottom).

The question remains if crosslink observations are solely sufficient to generate absolute navigation of a GEO and an LL_1 orbiter. Figure 4 illustrates the time series of the range and range-rate between assets in the Earth-Moon system. One can see that the range and range-rate between ground stations and the halo orbiter have less of a dynamic range than the range and range-rate between a GEO satellite and the halo orbiter. Hamilton and Melbourne describe the information content of a single pass of Doppler data between a ground station and a distant spacecraft.[20] The information content in a single pass between GEO and a distant spacecraft will be similar, except that the baseline distance is greater, which provides improved

geometry. Further, the GEO satellite remains in view of the Moon for much longer each day than a ground station does. It is very easy for a GEO satellite to obtain tracking data for low elevation angles relative to the Earth's surface since it is far from the Earth's surface. Therefore, it is expected that a GEO satellite's range or Doppler measurements of a satellite near the Moon will contain more information than a ground station's measurements. Analyses in Section V will study if the information content of this crosslink data truly has sufficient information to determine the absolute states of both satellites over time.

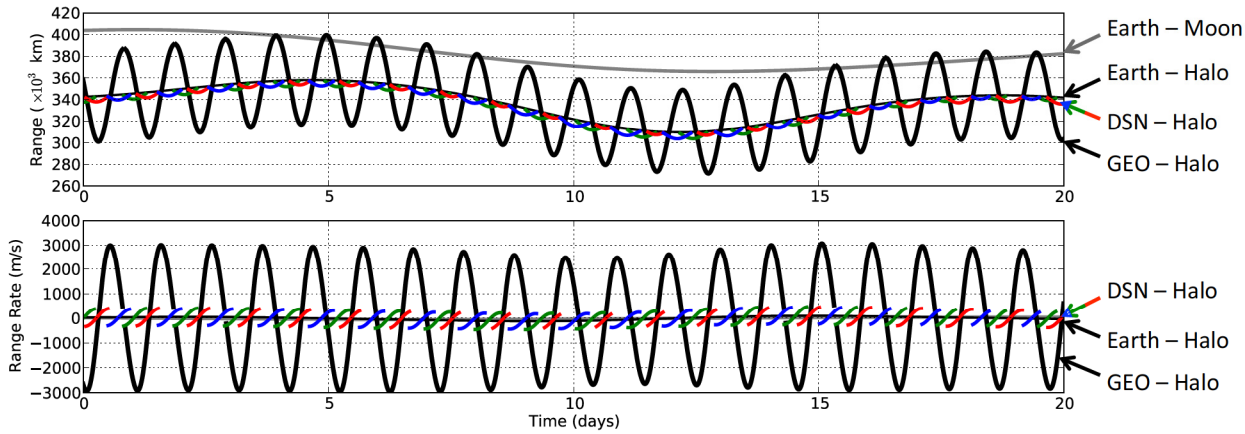

Figure 4. A comparison between ground-based and GEO-based observations of a satellite in orbit about the LL_1 point.

III. Mission Concept

A mission scenario is studied here that involves two satellites: one in a geosynchronous orbit about the Earth and another in a halo orbit about the Earth-Moon L_1 point. Two perspectives of this constellation are illustrated in Figure 1.

This particular application of LiAISON has many potential benefits. First, the lunar halo orbiter may be able to provide navigation services for many satellites in different GEO slots simultaneously, much like the GPS constellation for LEO orbiters. Current research is investigating the possibility of taking advantage of the GEO orbiters' side-lobes, so that the GEO satellites do not even have to point their communication antenna at the halo orbiter. The communication link may not close at all points in the GEO orbit, but concurrent research is demonstrating that only a few hours per orbit is more than sufficient to acquire good tracking.[9] Next, the geometrical information that the halo orbiter provides will significantly improve any tracking solution produced by ground stations. The halo orbiter is an asset that is not tied to the surface – it may be the only source of tracking data that has a variable geometry. Furthermore, the geometry sweeps out a wide range of angles each and every day as the GEO satellite moves about its orbit. Thus, the halo orbiter is in a great location to provide radial, in-track, and cross-track information about the GEO satellite's orbit.

A. Lunar L_1 Halo Orbit

The navigation satellite near the Moon is in a halo orbit about the Earth-Moon L_1 point, similar to the orbit that each of the Artemis spacecraft traversed in 2010 and 2011. The LL_1 point is one of five Lagrange points in the Earth-Moon system, namely, the five equilibrium points where the force of gravity of the Earth and Moon perfectly balance in a rotating coordinate system.[21] The LL_1 point is located between the Earth and the Moon, approximately 58,000 km from the Moon.

The Lagrange points, and libration orbits about them, are easily visualized and modeled in the circular restricted three-body problem (CRTBP).[21] The CRTBP models the motion of a massless particle, e.g., a spacecraft, in the presence of two massive bodies, e.g., the Earth and the Moon, where the two massive bodies are in circular orbits about their barycenter. The Moon's orbit about the Earth is near circular,

with an average eccentricity of about 0.05, which makes the CRTBP a reasonable model of the system. The analysis presented here uses values for the gravitational parameters of the Earth and Moon of 398,600.4415 km^3/s^2 and 4902.80 km^3/s^2, respectively. The distance between the two bodies is set to 384,410 km.

A convenient frame of reference in the CRTBP is the synodic reference frame: a frame that rotates with the motion of the two massive bodies. In the Earth-Moon system, the origin of the synodic frame is the barycenter, the x-axis points toward the Moon, the z-axis points in the direction of the angular momentum of the system, and the y-axis completes the right-handed coordinate frame. In this coordinate frame, the Earth, the Moon, and the five Lagrange points hold perfectly still.

Numerous periodic and quasi-periodic orbits exist in the CRTBP.[22–32] Some of the most studied orbits include the families of halo and Lissajous orbits about the collinear Lagrange points. Figure 5 illustrates several example Northern and Southern halo orbits about the Earth-Moon L_1 and L_2 points. One can see that a satellite in one of these orbits remains tied to the Lagrange point, but extends out of the Moon's orbital plane. Farquhar[33,34] and Clarke,[35] as well as more recent studies such as Hill, et al.,[3] have proposed using these orbits as locations for communication satellites at the Moon. It is apparent that a satellite in an orbit about L_2 has a continuous view of the far side of the Moon; in addition, satellites in Southern halo orbits have extended views of the lunar South Pole. The only drawback of these orbits is the extended link distance: a satellite in a libration orbit is typically around 60,000 km from the surface of the Moon.

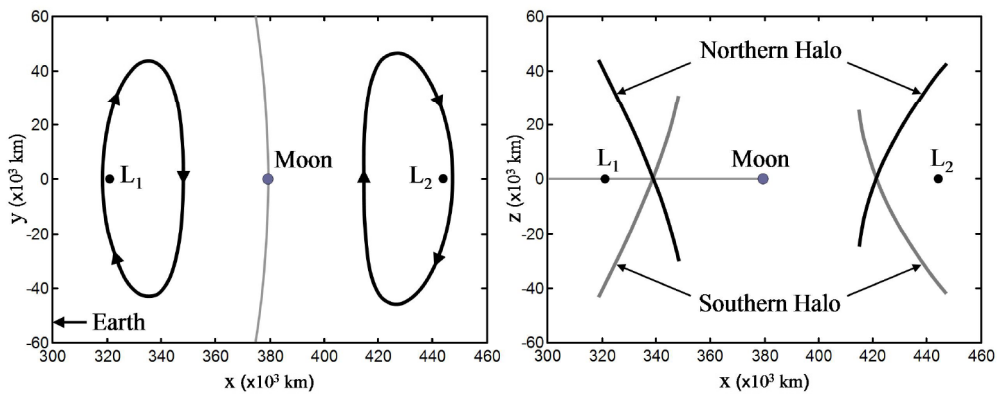

Figure 5. Example Northern and Southern halo orbits about the Earth-Moon L_1 and L_2 points, viewed from above (left) and the side (right) in the Earth-Moon rotating coordinate frame.[36]

The Lagrange points in the CRTBP hold fixed for all time. In the real solar system, the Lagrange points shift in position relative to the Earth and Moon, on account of the Moon's non-circular orbit about the Earth and other perturbations in the solar system. Similarly, a halo orbit in the CRTBP is perfectly periodic, whereas in the real solar system it never retraces its path. Figure 6 illustrates the difference between a halo orbit in the CRTBP and a similar quasi-halo orbit in a higher fidelity model of the solar system, generated using the Jet Propulsion Laboratory's DE405 Planetary and Lunar Ephemerides.[37]

A common procedure used to generate a quasi-halo orbit in a realistic model of the solar system, such as JPL's DE405 model, is to begin with an approximation and then differentially correct the trajectory in the higher fidelity model.[36,38] In this study, a series of states is generated using an analytic approximation of a halo orbit,[30,39] and those states are differentially corrected into the DE405 model using a multiple shooting differential corrector.[40,41] The result is a continuous trajectory in the realistic model of the solar system that closely approximates a halo orbit. Table 1 captures the parameters that have been used to generate the halo orbit used in the navigation simulations presented here.

B. Establishing the Lunar L_1 Halo Orbiter

It is possible to perform a direct transfer to place the L_1 orbiter in its orbit near the Moon, requiring a launch injection C_3 of approximately -2.0 km^2/s^2, a transfer duration of 3–5 days, and an orbit insertion maneuver of approximately 500 m/s.[36,42,43] Such a transfer is illustrated in Figure 7. Alternatively, the halo orbiter may be placed in its orbit using a low-energy lunar transfer. A low-energy transfer requires slightly

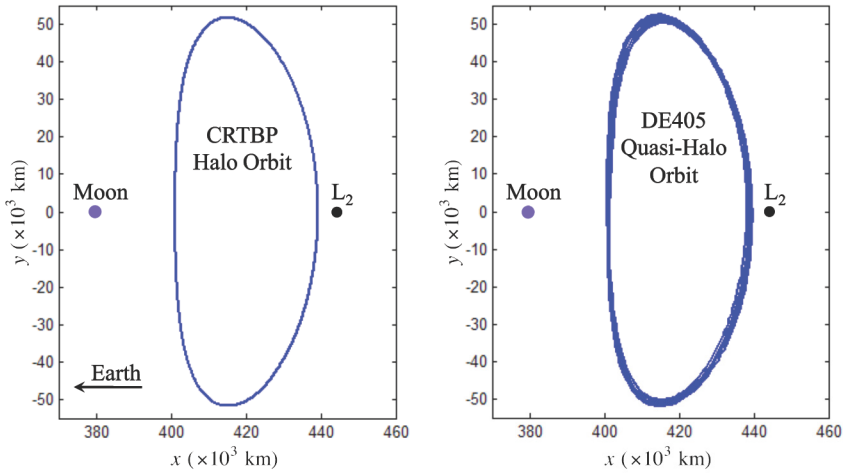

Figure 6. An example halo orbit about the Earth-Moon L_2 point generated in the CRTBP (left) and in the DE405 model of the solar system (right), viewed from above in the Earth-Moon rotating frame.

Table 1. The parameters of the L_1 quasi-halo orbit simulated here.

Parameter	Value	Comments
A_z	35,500 km	The z-axis amplitude
ϕ	0°	The initial phase angle of the orbit
t_{ref}	1/1/2020 00:00:00 ET	The reference epoch, ephemeris time

more energy at launch, namely, a C_3 of approximately -0.5 km^2/s^2, and a longer transfer duration of 80–120 days, but it removes all orbit insertion ΔV requirements, saving the spacecraft approximately 500 m/s of ΔV. An example low-energy trajectory from the Earth to the L_1 halo orbit is illustrated in Figure 8. This particular low-energy transfer arrives at the LL_2 vicinity approximately 91 days after its Earth departure maneuver and spends approximately 14 days traversing from LL_2 to LL_1 before inserting into the LL_1 halo orbit. It is ambiguous when the spacecraft *inserts* into the halo orbit since there is no required maneuver; for the purpose of this discussion the spacecraft has inserted once it has approached within 100 km of the halo reference trajectory.

C. The GEO Satellite

The GEO satellite simulated in this study is placed in a circular, equatorial orbit directly above a longitude of 0°. No station keeping is performed and it is assumed that the satellite can achieve a communication link with the halo orbiter well enough to collect range and range-rate observations.

IV. Orbit Determination

A. Theory

The process of orbit determination (OD) is useful for two purposes: to determine the best estimate of the state of a spacecraft at a particular time and to quantify the uncertainty in that state. Tapley, et al.,[44] provide a full description of the process of orbit determination; a brief overview will be presented here to place this study in context.

One typically begins with an initial guess for the state of a spacecraft at a reference epoch; the propagation of this state over time yields the spacecraft's *reference* trajectory. In reality, the spacecraft is not precisely following that trajectory, but is following a nearby trajectory, i.e., the *truth* trajectory. The process of orbit

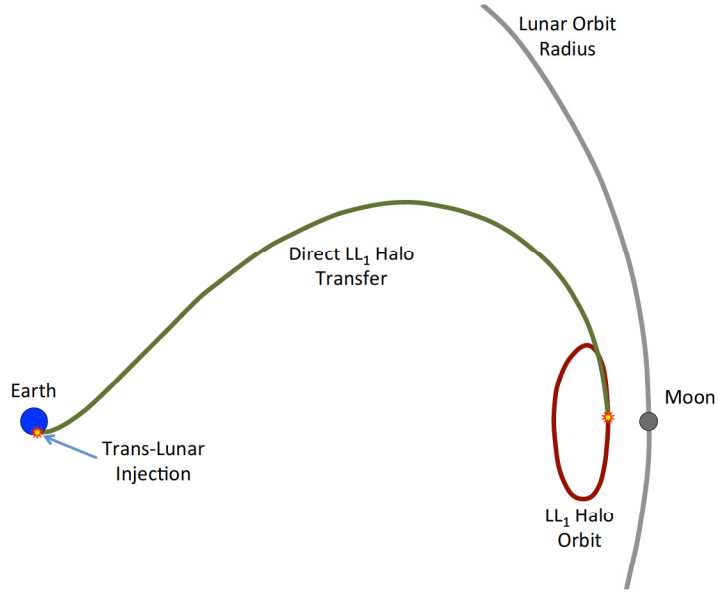

Figure 7. An example conventional halo transfer, which a satellite may follow to transfer to a lunar halo orbit within approximately six days. This transfer is viewed from above in the Earth-Moon rotating frame; the Moon's orbital radius is shown for reference.

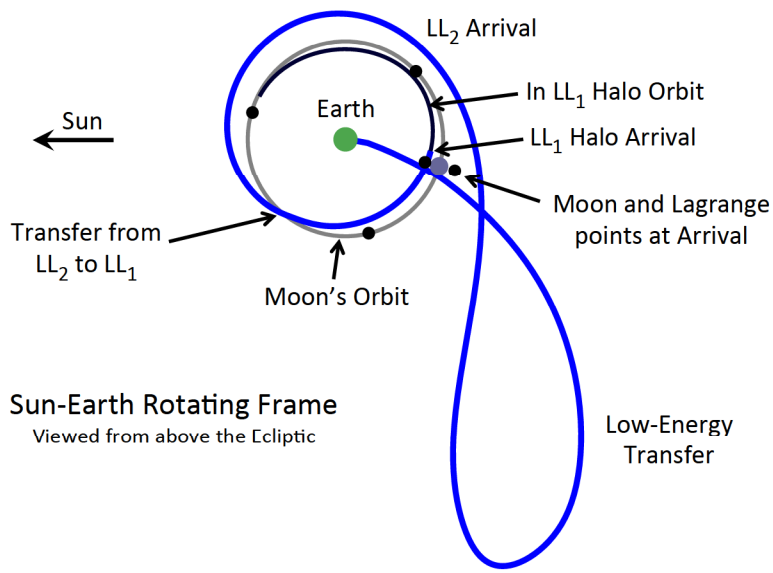

Figure 8. An example low-energy lunar halo transfer, which a satellite may follow to transfer to a lunar halo orbit for less ΔV than conventional transfers. This transfer is viewed from above in the Sun-Earth rotating frame.

determination takes a set of observations of the spacecraft, filters them, and determines a new estimate of the spacecraft's trajectory based on the reference trajectory to match the truth trajectory as well as possible.

The reference trajectory is propagated using a model that approximates the dynamics driving the truth trajectory. When performing OD on real spacecraft, the model is never perfect; the model is typically refined to capture the dynamics down to some acceptably small acceleration level.

Most spacecraft are tracked by ground stations or other satellites using one or several different measurement types. The studies presented here have generated sets of artificial tracking data that include

instantaneous range and range-rate measurements between the GEO satellite and the lunar halo orbiter. Realistic observations must account for the time it takes to transmit, receive, and process measurements, as well as converting a Doppler observation into a range-rate measurement.

The process of orbit determination takes a large set of observations, each of which includes errors, and processes them all to statistically determine the best estimate of the spacecraft's trajectory. Each observed measurement is compared to the expected observation, given the current best estimate of the spacecraft's trajectory. The observed measurement minus the expected measurement yields a *residual*. The goal of the OD process is to determine the initial state of the spacecraft that minimizes the residuals using some cost function. The most common cost function is the sum of the squares of each residual.

Before processing any observations, one must first establish an initial covariance matrix. The covariance matrix captures the estimate of the uncertainty of each state variable at the reference epoch. The covariance will change as measurements are processed, reflecting the additional knowledge provided by those measurements. If the current estimate of the trajectory is good and the measurements do not have large errors, then the covariance matrix will shrink, indicating an increased confidence in the state estimate.

Several algorithms are commonly used to process measurements during the orbit determination process. A *batch* processor operates on all of the observations simultaneously, weighing each observation the same as any other. When the batch processor has converged, it provides a best estimate for the state of the spacecraft at the reference epoch and a covariance matrix to go with it. The state and covariance matrix may then be mapped to any other time.

The conventional Kalman filter (CKF), or *sequential* filter behaves much like the batch processor, but it operates on one measurement at a time instead of all measurements simultaneously. Thus, the CKF begins with an initial estimate of the state and an initial covariance matrix at the reference epoch and then maps them forward in time from one measurement to the next. As each observation is processed, the covariance matrix shrinks or grows, depending on the system. The CKF and batch processor generate consistent results for systems that have continuous dynamics..

The extended Kalman filter (EKF) is a variation of the CKF. As the EKF processes an observation, it updates the reference trajectory using that observation. The update is proportional to the current covariance matrix. That is, if many observations have been processed and the covariance has shrunk (indicating a good trajectory fit), and an observation is then processed with a large residual, the reference trajectory will not be adjusted much. But if the covariance is large, the trajectory may be adjusted more significantly. The EKF is typically only stable after a sufficient number of observations have been processed with the CKF.

B. OD Implementation

1. *The State Vector*

The orbit determination process begins by selecting a set of state variables, namely the unknown variables of interest. The state vector $\mathbf{X}$ in this study contains 12 variables: the positions and velocities of the GEO and halo orbiters:

$$\mathbf{X} = [\ x_g,\ y_g,\ z_g,\ \dot{x}_g,\ \dot{y}_g,\ \dot{z}_g,\ x_h,\ y_h,\ z_h,\ \dot{x}_h,\ \dot{y}_h,\ \dot{z}_h\ ]^T\ ,$$

where the g subscript corresponds to the GEO satellite and the h subscript corresponds to the halo orbiter. Other common state variables include the coefficient of reflectivity of each satellite, components of maneuver executions, measurement bias values, clock offsets, etc. Some of these are included in an advanced study of this scenario.[9]

2. *State Dynamics*

The state vector varies in time and may be written in the simple dynamical form:

$$\dot{\mathbf{X}}(t) = \boldsymbol{f}(t, \mathbf{X}(t)). \tag{1}$$

The state vector is used to generate a reference trajectory that is near the truth trajectory. This study considers scenarios in both the CRTBP and in the full ephemeris model of the solar system, using the standard equations of motion for both systems.[21,36] In the CRTBP, the truth dynamics are identical to the reference dynamics. In the full ephemeris model of the solar system, the truth dynamics include point-mass gravity potentials for the Sun, Moon, and all of the planets, whereas the reference dynamics only include point-mass gravity potentials for the Sun, Earth, and Moon. This introduces some dynamical errors.

The state's propagation over time must be performed using a numerical integrator. In this study, the integration has been performed using a Runge-Kutta DOPRI8(7)13 integrator[45] with variable step size control using a relative step tolerance of 10^{-14}.

3. *Measurements*

Simulated *observed* measurements have been generated for this study by taking the states of the GEO and halo satellites along the truth trajectories and computing instantaneous range and range-rate values at each measurement time. The measurements are then corrupted by adding a constant bias and a Gaussian white-noise. The bias represents errors in modeling the path of the signal through each antenna, which remain fairly constant throughout any given observation arc. The white-noise corresponds to errors that fluctuate frequently, such as temperature shifts, oscillator errors, clock errors, etc. The white-noise component is taken from a Gaussian distribution with zero mean and a given standard deviation. The observed measurements are given as:

$$\mathbf{Y}_O(t) = \boldsymbol{h}(t, \mathbf{X}(t)) + \boldsymbol{\nu} = \begin{bmatrix} \rho(t) + \rho_{\text{bias}} + \rho_{\text{noise}} \\ \dot{\rho}(t) + \dot{\rho}_{\text{bias}} + \dot{\rho}_{\text{noise}} \end{bmatrix}. \tag{2}$$

Equation 2 may be related to the state vector variables via the following relationships, where these values are all computed at some measurement time:

$$\rho = \sqrt{\left(x_h - x_g\right)^2 + \left(y_h - y_g\right)^2 + \left(z_h - z_g\right)^2} \tag{3}$$

$$\dot{\rho} = \frac{\left(x_h - x_g\right)\left(\dot{x}_h - \dot{x}_g\right) + \left(y_h - y_g\right)\left(\dot{y}_h - \dot{y}_g\right) + \left(z_h - z_g\right)\left(\dot{z}_h - \dot{z}_g\right)}{\sqrt{\left(x_h - x_g\right)^2 + \left(y_h - y_g\right)^2 + \left(z_h - z_g\right)^2}} \tag{4}$$

When a reference trajectory is generated, a set of *computed* measurements are simulated by taking the states of each satellite along the reference trajectory and computing the instantaneous range and range-rate between them. The difference between the observed and computed measurements is equal to ϵ:

$$\epsilon = \mathbf{Y}_O - \mathbf{Y}_C. \tag{5}$$

The standard cost function, J, is then computed using a least-squares formulation:

$$J = 1/2\epsilon^T\epsilon. \tag{6}$$

4. *State Mappings*

The OD process must be able to characterize how to change the initial state of the estimated trajectory in order to better fit the measurement residuals and reduce the cost function J. Hence, the process requires information about how to map a measurement residual back to the initial state vector. This mapping is accomplished by linearizing the state dynamics about a reference trajectory. If $\mathbf{X}^*(t)$ is a reference trajectory near the truth trajectory, then we can define a state deviation vector $\mathbf{x}(t)$ to be:

$$\mathbf{x}(t) = \mathbf{X}(t) - \mathbf{X}^*(t). \tag{7}$$

The *a priori* state deviation vector is then $\overline{\mathbf{x}}(t)$, generated from an *a priori* state estimate at the reference epoch $\overline{\mathbf{X}}(t_0)$. The goal of the OD process is to compute an estimated correction to the state vector $\hat{\mathbf{x}}(t)$, such that the resulting trajectory generated by a new state $\hat{\mathbf{X}}(t_0) = \mathbf{X}(t_0) + \hat{\mathbf{x}}(t_0)$ reduces the measurement residual cost function (Equation 6).

The state transition matrix, Φ, may be used to map the state deviation vector from one time to another via the following partials:

$$\Phi(t_2, t_1) = \frac{\partial \mathbf{X}(t_2)}{\partial \mathbf{X}(t_1)}, \tag{8}$$

permitting the state deviation mapping:

$$\mathbf{x}(t_2) = \Phi(t_2, t_1)\mathbf{x}(t_1). \tag{9}$$

The state transition matrix may be used to map forward or backward in time, such that

$$\Phi(t_2, t_1) = \Phi(t_1, t_2)^{-1}. \tag{10}$$

The state transition matrix may be constructed any time the reference trajectory is integrated by integrating the following equation simultaneously:

$$\dot{\Phi}(t, t_0) = A(t)\Phi(t, t_0), \tag{11}$$

with initial condition $\Phi(t_0, t_0) = I$. The matrix $A(t)$ is equal to:

$$A(t) = \frac{\partial \boldsymbol{f}(t, \mathbf{X}(t))}{\partial \mathbf{X}(t)} = \frac{\partial \dot{\mathbf{X}}(t)}{\partial \mathbf{X}(t)}. \tag{12}$$

In this study, the $A(t)$ matrix is composed of the following pieces:

$$A(t) = \begin{bmatrix} \frac{\partial \dot{\mathbf{r}}_g(t)}{\partial \mathbf{r}_g(t)} & \frac{\partial \dot{\mathbf{r}}_g(t)}{\partial \dot{\mathbf{r}}_g(t)} & \frac{\partial \dot{\mathbf{r}}_g(t)}{\partial \mathbf{r}_h(t)} & \frac{\partial \dot{\mathbf{r}}_g(t)}{\partial \dot{\mathbf{r}}_h(t)} \\ \frac{\partial \ddot{\mathbf{r}}_g(t)}{\partial \mathbf{r}_g(t)} & \frac{\partial \ddot{\mathbf{r}}_g(t)}{\partial \dot{\mathbf{r}}_g(t)} & \frac{\partial \ddot{\mathbf{r}}_g(t)}{\partial \mathbf{r}_h(t)} & \frac{\partial \ddot{\mathbf{r}}_g(t)}{\partial \dot{\mathbf{r}}_h(t)} \\ \frac{\partial \dot{\mathbf{r}}_h(t)}{\partial \mathbf{r}_g(t)} & \frac{\partial \dot{\mathbf{r}}_h(t)}{\partial \dot{\mathbf{r}}_g(t)} & \frac{\partial \dot{\mathbf{r}}_h(t)}{\partial \mathbf{r}_h(t)} & \frac{\partial \dot{\mathbf{r}}_h(t)}{\partial \dot{\mathbf{r}}_h(t)} \\ \frac{\partial \ddot{\mathbf{r}}_h(t)}{\partial \mathbf{r}_g(t)} & \frac{\partial \ddot{\mathbf{r}}_h(t)}{\partial \dot{\mathbf{r}}_g(t)} & \frac{\partial \ddot{\mathbf{r}}_h(t)}{\partial \mathbf{r}_h(t)} & \frac{\partial \ddot{\mathbf{r}}_h(t)}{\partial \dot{\mathbf{r}}_h(t)} \end{bmatrix} = \begin{bmatrix} \mathbf{0} & \mathbf{I} & \mathbf{0} & \mathbf{0} \\ \frac{\partial \ddot{\mathbf{r}}_g(t)}{\partial \mathbf{r}_g(t)} & \frac{\partial \ddot{\mathbf{r}}_g(t)}{\partial \dot{\mathbf{r}}_g(t)} & \mathbf{0} & \mathbf{0} \\ \mathbf{0} & \mathbf{0} & \mathbf{0} & \mathbf{I} \\ \mathbf{0} & \mathbf{0} & \frac{\partial \ddot{\mathbf{r}}_h(t)}{\partial \mathbf{r}_h(t)} & \frac{\partial \ddot{\mathbf{r}}_h(t)}{\partial \dot{\mathbf{r}}_h(t)} \end{bmatrix}. \tag{13}$$

The simplifications shown are valid for the simulations presented here, since there are no dependencies on the propagation of either satellite on the state of the other. The other relationships must be computed for any given dynamical model.

5. *Measurement Mappings*

One can construct a linearized observation deviation vector $\mathbf{y}$ in much the same way as the state deviation vector. The goal is to express the observation deviation vector as a function of the state deviation vector at the reference epoch, namely:

$$\mathbf{y}(t) = H(t)\mathbf{x}(t_0) + \epsilon(t), \tag{14}$$

where $H(t)$ is the measurement mapping matrix and $\epsilon(t)$ is the observation noise at the time of the measurement. Using Equation 9, this relationship may be simplified to a mapping of the observation deviation vector to the state deviation vector at the same time:

$$\mathbf{y}(t) = H(t)\Phi(t_0, t)\mathbf{x}(t) + \epsilon(t). \tag{15}$$

If we then use Equation 10 and the definition

$$H(t) = \tilde{H}(t)\Phi(t, t_0), \tag{16}$$

then Equation 15 becomes:

$$\mathbf{y}(\iota) = \tilde{H}(\iota)\mathbf{x}(\iota) + \epsilon(\iota). \tag{17}$$

The mapping matrix $\tilde{H}(t)$ is constructed via the following partials:

$$\tilde{H}(t) = \frac{\partial \boldsymbol{h}(t, \mathbf{X}(t))}{\partial \mathbf{X}(t)}. \tag{18}$$

In this study, the following simplifications may be made, considering the dependencies given in Equations 3 and 4. The remainder of the partials are not shown here for brevity.

$$\tilde{H}(t) = \begin{bmatrix} \frac{\partial \rho(t)}{\partial \mathbf{r}_g(t)} & \mathbf{0} & \frac{\partial \rho(t)}{\partial \mathbf{r}_h(t)} & \mathbf{0} \\ \frac{\partial \dot{\rho}(t)}{\partial \mathbf{r}_g(t)} & \frac{\partial \dot{\rho}(t)}{\partial \dot{\mathbf{r}}_g(t)} & \frac{\partial \dot{\rho}(t)}{\partial \mathbf{r}_h(t)} & \frac{\partial \dot{\rho}(t)}{\partial \dot{\mathbf{r}}_h(t)} \end{bmatrix}. \tag{19}$$

6. *The Batch Processor*

The batch processor accumulates numerous observations and processes them all simultaneously to produce a correction to the state at the reference epoch. Since the mappings given above have been linearized about the reference trajectory, the correction may not generate the optimal state. Hence, the algorithm is often iterated until the correction is sufficiently small: typically only two or three times.

The best estimate for the state deviation vector at the reference epoch $\hat{\mathbf{x}}(t_0)$ is computed by solving the normal equations:

$$\mathbf{\Lambda}\hat{\mathbf{x}}(t_0) = \boldsymbol{N}, \tag{20}$$

where $\mathbf{\Lambda}$ and $\boldsymbol{N}$ are accumulated from every observation i in the following manner:

$$\mathbf{\Lambda} = \overline{P}_0^{-1} + \sum_i H_i^T W_i H_i \tag{21}$$

$$\boldsymbol{N} = \overline{P}_0^{-1}\overline{x}_0 + \sum_i H_i^T W_i y_i \tag{22}$$

The best estimate state deviation vector $\hat{\mathbf{x}}(t_0)$ is then added to the estimated state at the reference epoch. In these equations $\overline{P}_0$ is the *a prior* variance-covariance matrix and W is the measurement weighting matrix.

7. *Conventional Kalman Filter*

The conventional Kalman filter generates an estimate for the state in the same manner as the batch processor, but rather than processing all of the data simultaneously, the CKF processes one observation at a time. The benefit is that rather than inverting one large matrix, the CKF inverts many small matrices. For the study presented here, the conventional Kalman filter will generate the same estimate of the state in the presence of perfect mathematics. However, machine precision changes the accuracy of the estimation.

The CKF begins with an *a prior* state estimate $\mathbf{X}_0$ with $\overline{\mathbf{x}}_0 = \mathbf{0}$, an *a priori* covariance matrix $\overline{P}_0$, and a measurement weighting matrix W. It then either maps these forward in time to the first observation or processes an observation at the initial time. If there is no observation, then $\hat{\mathbf{x}}_0 = \overline{\mathbf{x}}_0$ and $P_0 = \overline{P}_0$. The CKF then moves through the observations one at a time performing two steps: the *Time Update*, which propagates the state estimate and covariance to the next observation time, and the *Measurement Update*, which updates the best estimate of the state deviation vector and covariance given the observation at that time.

The Time Update equations include:

$$\overline{\mathbf{x}}_i = \Phi(t_i, t_{i-1})\hat{\mathbf{x}}_{i-1} \tag{23}$$

$$\overline{P}_i = \Phi(t_i, t_{i-1})P_{i-1}\Phi(t_i, t_{i-1})^T \tag{24}$$

The Measurement Update equations include:

$$K_i = \overline{P}_i\tilde{H}_i^T\left(\tilde{H}_i\overline{P}_i\tilde{H}_i^T + W_i^{-1}\right)^{-1} \tag{25}$$

$$\hat{\mathbf{x}}_i = \overline{\mathbf{x}}_i + K_i\left(y_i - \tilde{H}_i\overline{\mathbf{x}}_i\right) \tag{26}$$

$$P_i = \left(I - K_i\tilde{H}_i\right)\overline{P}_i \tag{27}$$

After the final observation has been processed, then the final best estimate state deviation vector is mapped back to the reference epoch and added to the reference state vector:

$$\hat{\mathbf{X}}(t_0) = \mathbf{X}(t_0) + \Phi(t_0, t_f)\hat{\mathbf{x}}(t_f). \tag{28}$$

There are various techniques available to help the numerical stability of the algorithm. For instance, the Joseph formulation may be used to prevent the covariance matrix from losing its symmetric condition:

$$P_i = (I - K_i\tilde{H}_i)\overline{P}_i(I - K_i\tilde{H}_i)^T + K_iW_i^{-1}K_i^T. \tag{29}$$

One advantage of sequential algorithms such as the CKF is that it generates an update to the variance-covariance matrix at every observation, which provides information about how the process is behaving.

8. *Extended Kalman Filter*

The extended Kalman filter is a variation of the conventional Kalman filter. Where the CKF used the final best estimate state deviation vector to update the reference state vector in Equation 28, the EKF updates the state at each measurement update. Because of this, the state transition matrix cannot be pre-computed, but must be generated at the time that it is needed. Another consequence of this filter is that if the covariance matrix is too large, the reference trajectory risks departing from the truth trajectory such that the filter will diverge. A common strategy is to process the first portion of observations using a CKF until the covariance has shrunk, and then switch to the EKF.

9. *Process Noise*

One way that the Kalman filter fails is by saturating the filter. If the covariance matrix shrinks too much, future observations will not impact the estimate of the state. This can be particularly troublesome if the dynamics depend on a gradually changing geometry to make each state variable observable, e.g., as the halo orbit gradually moves around its orbit. One can insert process noise into the filter in order to keep the covariance matrix large enough such that all observations influence the estimate.

Process noise is injected into Equation 1 as follows:

$$\dot{\mathbf{X}}(t) = \boldsymbol{f}(t, \mathbf{X}(t), \mathbf{u}(t)), \tag{30}$$

where $\mathbf{u}(t)$ is a zero-mean Gaussian white noise vector. The process noise transition matrix is constructed much like the state transition matrix:

$$\Gamma(t_2, t_1) = \frac{\partial \mathbf{X}(t_2)}{\partial \mathbf{u}(t_1)}, \tag{31}$$

and Equation 9 is updated to include process noise as follows:

$$\mathbf{x}(t_2) = \Phi(t_2, t_1)\mathbf{x}(t_1) + \Gamma(t_2, t_1)\mathbf{u}(t_1). \tag{32}$$

The process noise covariance matrix $Q(t)$ is introduced to the Kalman filter as a means of inflating the covariance matrix. One first specifies an *a priori* matrix $\overline{Q}(t)$, which is typically a diagonal matrix with specified σ values along the diagonal. Equation 24 is updated to include process noise:

$$\overline{P}_i = \Phi(t_i, t_{i-1})P_{i-1}\Phi(t_i, t_{i-1})^T + \overline{Q}_{i-1}. \tag{33}$$

The process noise covariance matrix is mapped through time much like the variance-covariance matrix:

$$\overline{Q}_i = \Gamma(t_i, t_{i-1})Q_{i-1}\Gamma(t_i, t_{i-1})^T. \tag{34}$$

In this study, $\Gamma(t_i, t_{i-1})$ is a function of the duration of time since the last observation, $\Delta t = t_i - t_{i-1}$:

$$\Gamma(t_i, t_{i-1}) = \begin{bmatrix} \Delta t^2/2 \times \mathbf{I}_{3\times 3} \\ \Delta t/2 \times \mathbf{I}_{3\times 3} \end{bmatrix}. \tag{35}$$

C. Cramér-Rao Lower Bound

With so many orbit determination filter options and tuning parameters available, particularly with sequential algorithms, it may not be obvious when an optimal OD configuration has been constructed. The Cramér-Rao Lower Bound (CRLB) or Cramér-Rao inequality may be computed to measure the lower bound on the uncertainty that a particular unbiased estimator may achieve if it is optimal.[46–49] If one's OD filter is achieving an uncertainty in its estimates near the CRLB, then no further optimizations are necessary. Conversely, if one's results are far worse than the CRLB, then it may be useful to continue tuning the filter to achieve less uncertainty in the results.

If P is the estimation error covariance matrix that corresponds to any unbiased estimator of the unknown state parameters, and P^* is the CRLB, then one may state:

$$P \geq P^* \equiv J^{-1},$$

where J is the Fisher information matrix. Fortunately it is straightforward to compute P^* for an EKF statistical orbit determination filter.[49] Taylor proved the following proposition:[49]

Proposition: The inverse Fisher information matrix (P^*) corresponding to a dynamic system modeled by a nonlinear time-varying state vector differential equation with deterministic inputs and nonlinear time-varying observations of the state variables corrupted by additive Gaussian white noise sequences propagates according to the same equations as the filter covariance matrix for an extended Kalman filter (EKF) linearized about the true (unknown) trajectory.

Hence, the only main differences between the EKF statistical orbit determination process summarized above and the computation of the CRLB is that the CRLB uses the true trajectory rather than the current reference trajectory, which is only available in simulations, and the CRLB analysis includes no process noise.

Computationally, one generates the P^* matrix at each instant of time by first initializing the matrix at the reference epoch:

$$P^*(t_0) = \overline{P}_0^{-1},$$

and then one iterates the following equation at each time update:

$$P^*(t_k)^{-1} = \left(\Phi(t_k, t_{k-1})P^*(t_{k-1})\Phi(t_k, t_{k-1})^T\right)^{-1} + H(t_k)^T W(t_k) H(t_k),$$

such that the truth trajectory is used rather than the reference trajectory.

V. Navigation Simulations

Several simulations have been performed to demonstrate that the relative satellite-to-satellite measurements between a GEO satellite and a lunar libration orbiter can achieve absolute orbital navigation as well as relative navigation of both satellites. First, a covariance study, i.e., a Cramér Rao Lower Bound analysis, has been performed in the CRTBP to illustrate that the absolute geometry is indeed observable. Then a navigation simulation has been conducted, implementing an extended Kalman filter for the OD estimator, again in the simple CRTBP. The scenarios have been converted to a higher fidelity model of the solar system and repeated to illustrate LiAISON's results in a realistic model of the solar system. Finally, the results have been modeled in the Jet Propulsion Laboratory's navigation software suite MONTE (Mission-analysis, Operations, and Navigation Toolkit Environment) to validate the developed software.

Each of the simulations uses instantaneous range and range-rate observations between the GEO satellite and the lunar libration orbiter, once every 100 seconds. The observations have 1 meter and 1 cm/s (1-σ) white noise applied. The state includes the 12 position and velocity components of both satellites. Unless otherwise noted, the *a priori* covariance matrix has been set to be diagonal with 1-σ standard deviation values set to 100 meters in position and 0.1 m/s in velocity.

The results of these simulations have been very promising; enough to warrant a concurrent study that has explored the trade studies involved with high-fidelity simulations.[9] The simulations include modeling errors of every aspect of the dynamical model and a more realistic schedule of observations. Nevertheless, the simulations conducted in this study demonstrate that LiAISON is indeed a viable method to obtain absolute measurements of the two satellite orbits using crosslink observations.

A. Simulating in the CRTBP

This section describes the results of the simulations performed in the CRTBP. The dynamical model includes only the force of gravity of a point-mass Earth and a point-mass Moon in circular orbits about their barycenter. The advantage of studying this model is that the navigation process cannot take advantage of any recognizable perturbations that may exist in a real system, such as a near-constant solar radiation pressure, or even the gravitational attraction of the Sun.

The initial conditions $(x_0, y_0, z_0, \dot{x}_0, \dot{y}_0, \dot{z}_0)$ of the two satellites in the Earth-Moon barycentric rotating frame are given as:

L_1 Halo: Position: (3.18286×10^5 km, 0 km, 3.84410×10^4 km),
Velocity: (0 km/s, 2.20731×10^{-1} km/s, 0 km/s).

GEO: Position: (-4.58570×10^3 km, -4.21560×10^4 km, 2.67875×10^3 km),
Velocity: (2.95332×10^0 km/s, 6.03254×10^{-3} km/s, -1.94804×10^{-1} km/s).

These conditions yield the trajectories for a satellite in a circular, equatorial geostationary orbit and a satellite in a halo orbit about the Earth-Moon L_1 point.

B. Cramér Rao Lower Bound Analysis

A Cramér Rao Lower Bound analysis has been performed on the crosslink observations of this two-satellite constellation in order to measure how observable the states of each satellite are in this scenario. The *a priori* covariance has been set very high: to a diagonal matrix with values of 10^{20} on the diagonal. The weighting matrix has been set to reflect the uncertainty in the observations, namely, 1 meter for the range observations and 1 mm/s for the range-rate observations. Figure 9 illustrates the position and velocity components of the resulting variance-covariance matrix as observations are processed. One can see that the position and velocity uncertainties of both satellites falls to approximately the state of the art in satellite navigation after about three days of tracking, i.e., to approximately 100 meters and 10 meters in position for the halo and GEO satellites, respectively, and to approximately 1 mm/s in velocity for the two satellites. The uncertainty continues to fall until it reaches an approximate steady-state after approximately 10 days of tracking. The final steady-state uncertainty is below 1 meter in position for both satellites and below 0.01 mm/s and 0.1 mm/s in velocity for the halo and GEO satellites, respectively.

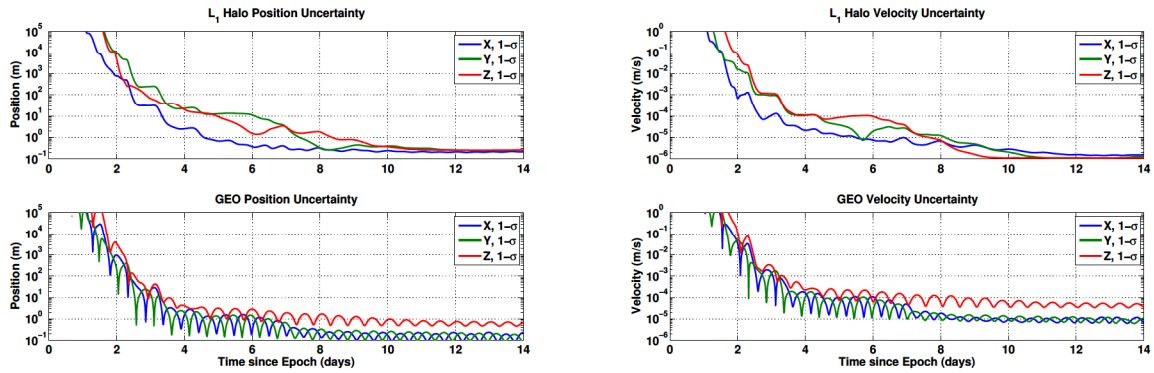

Figure 9. Time evolution of the position (left) and velocity (right) components of the covariance matrix, resulting from the Cramér Rao Lower Bound analysis in the CRTBP. The coordinates are specified in the Earth-Moon synodic coordinate frame.

One notices that the z-axis uncertainty of the GEO satellite is greater than the in-plane components. This may be explained because the out-of-plane geometry is less observable than the in-plane geometry. This simulation involves about a 23° difference in the plane of the GEO orbiter and the Moon's orbital plane. If that difference were close to zero, then there would be very little information about the out-of-plane motion. Hence, one can expect to see a relationship between the accuracy of the out-of-plane motion relative to the accuracy of the in-plane motion to be on the order of the cosine of 23 degrees divided by the sine of 23 degrees. This results in an expected z-axis uncertainty amplitude about 2.4 times larger than the in-plane uncertainty amplitude, which is roughly what is seen in Figure 9.

This analysis has been repeated for range-only data as well as for range and range-rate data. The results are nearly identical, though the range-rate data improves the uncertainty early on. The steady-state values are approximately equal.

Hill introduced a cost function known as β_{ave} to evaluate the quality of a solution.[6] The parameter is determined by computing the mean of the temporal average of the maximum 3-σ position error ellipsoid axis for both satellites. A small β_{ave} indicates that the covariance has reduced, or, that the uncertainty in the state parameters has fallen, and thus the observations contain information regarding each parameter in the satellites' state. The simulation presented here results in a β_{ave} value of approximately 0.6 meters, meaning that the maximum 3-σ position error ellipsoid for both satellites is below 1 meter. Indeed, the state parameters are observable.

This simulation has been repeated using different initial conditions for both the GEO orbiter and the halo orbiter. The halo orbiter has been initialized at three different locations in its orbit, namely, at τ-values of 0°, 90°, and 180°, where τ is a parameter analogous to a conic orbit's mean anomaly.[36] The GEO orbiter begins at many different points about its orbit. The results are extremely consistent. The β_{ave}-values for every simulation existed in the interval 0.590221 meters $\leq \beta_{\text{ave}} \leq$ 0.658240 meters. The 3-σ uncertainty in the position of both satellites always falls to approximately 0.6 meters.

This analysis illustrates that the state variables are indeed observable using just crosslink data in the pres-

ence of no asymmetric forces except what is present in the CRTBP. Presumably the addition of asymmetric forces and ground-based tracking would help accelerate the convergence.

C. Navigation Simulation

The next step is to process simulated range measurements between the GEO satellite and the L_1 halo orbiter using a Kalman filter. The GEO and halo states given above have been used as the truth trajectories and deviations in those states have been used as the reference trajectories. The initial state deviation is 100 meters in position and 1 cm/s in velocity for both satellites. The *a priori* covariance is set to correspond with the initial state deviation: it has been set to a diagonal matrix with values of 10^4 m^2 in position and 10^{-2} (m/s)^2 in velocity for both satellites. State noise compensation has been implemented with a σ value of 1×10^{-13} m/s^2 for the halo orbiter and 1×10^{-14} m/s^2 for the GEO satellite on the diagonal of the *a priori* process noise covariance matrix. After exploring several scenarios, it has been determined that the simulation with the best convergence properties is one that uses an extended Kalman filter starting with the first observation. No observations are processed at all with a conventional Kalman filter.

Figure 10 illustrates the time evolution of the position and velocity accuracy of the simulation as the EKF processes the observations, namely, the difference between the truth trajectory and the estimated trajectory over time. Figure 11 presents the components of the covariance matrix over time on a logarithmic axis for clarity. One can see that the uncertainty of the position of either satellite converges to about one meter within about eight days. The coordinates are represented in the Earth-Moon rotating coordinate frame. The increased z-axis uncertainty is again noticeable, and corresponds again to an increased uncertainty by a factor of approximately 2.4. The largest off-diagonal element in the variance-covariance matrix after 9 days of processing has a value of approximately 1.1×10^{-17}, illustrating that there is no correlation in the state variables. The post-fit range residuals have an RMS of approximately 0.99519 meters.

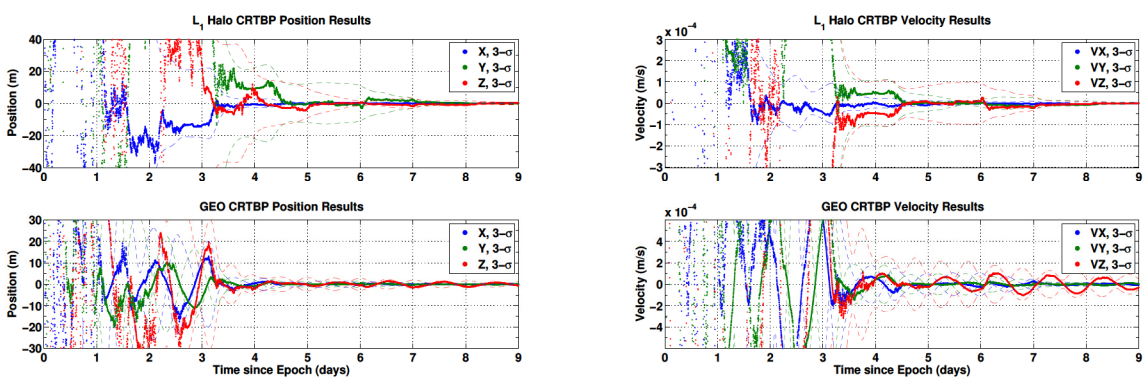

Figure 10. Time evolution of position (left) and velocity (right) accuracy (truth − estimate) plotted with 3-σ covariance envelopes (dotted lines). Top plot is for the L_1 halo orbiter and the bottom is for the GEO satellite. The coordinates are given in the Earth-Moon synodic reference frame in the CRTBP.

D. Full Ephemeris

In this section, the analysis is extended to a more dynamically complex and realistic scenario, where the satellites are propagated in the presence of all of the planets and the Moon and the positions of each body are modeled using the JPL Developmental Ephemerides DE405.[37] In this model, the L_1 orbiter is not in a perfectly periodic orbit, as described above. Every filter parameter has been set to be identical to the CRTBP scenario in order to directly compare them.

Figure 12 illustrates the time evolution of the position and velocity accuracy of the simulation as the EKF processes the observations, namely, the difference between the truth trajectory and the estimated trajectory over time. Figure 13 presents the components of the covariance matrix over time on a logarithmic axis for clarity. The components in each figure are in the Geocentric Celestial Reference Frame (GCRF), the Earth-centered version of the ICRF.[50] The z-axis is approximately aligned with the Earth's spin axis, and the other axes are approximately aligned with the equatorial plane. One can see that the uncertainty of the position of either satellite converges to about one meter within about seven days: somewhat faster than the

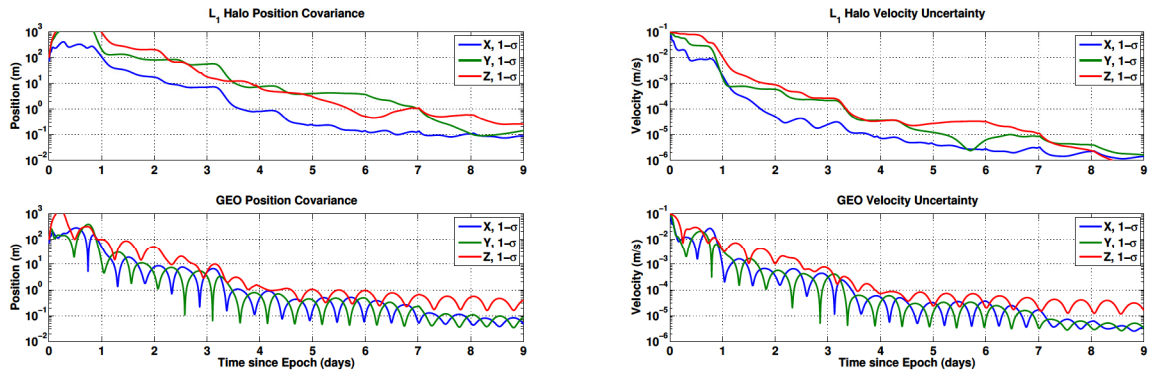

Figure 11. Time evolution of the position and velocity variance for the two satellites in the CRTBP.

convergence in the CRTBP. The largest off-diagonal element in the variance-covariance matrix after 9 days of processing has a value of approximately 0.0054, quite a bit larger than largest covariance in the CRTBP's simulation. Still, the correlation is small between all state variables.

Finally, Figure 14 illustrates the residuals after the state has been updated. One can see that the residuals have an RMS of approximately 1 meter and 1 mm/s, again corresponding with the level of noise applied to the observations.

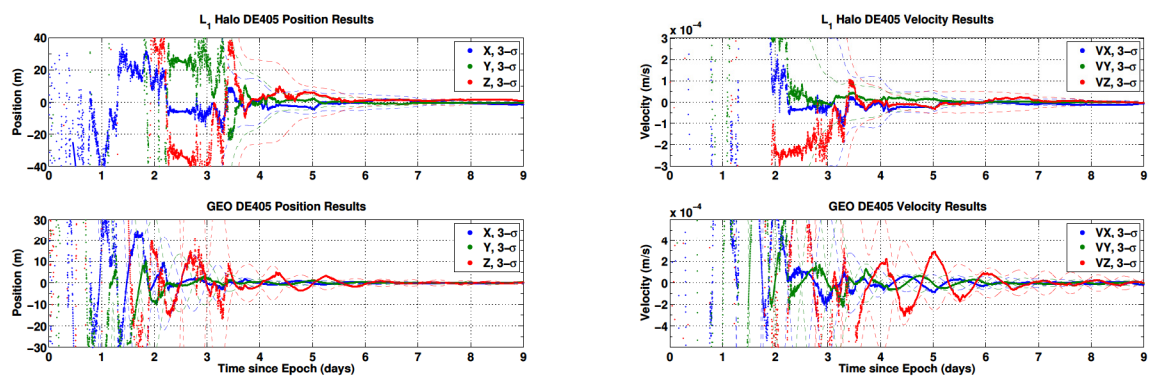

Figure 12. Time evolution of position (left) and velocity (right) accuracy (truth − estimate) plotted with 3-σ covariance envelopes (dotted lines). Top plot is for the L_1 halo orbiter and the bottom is for the GEO satellite. The coordinates are given in GCRF.

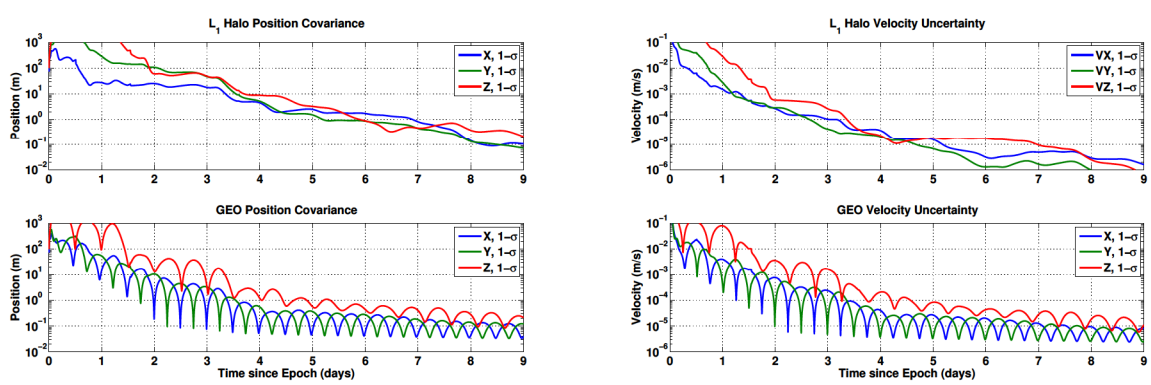

Figure 13. Time evolution of the position and velocity variance for the two satellites.

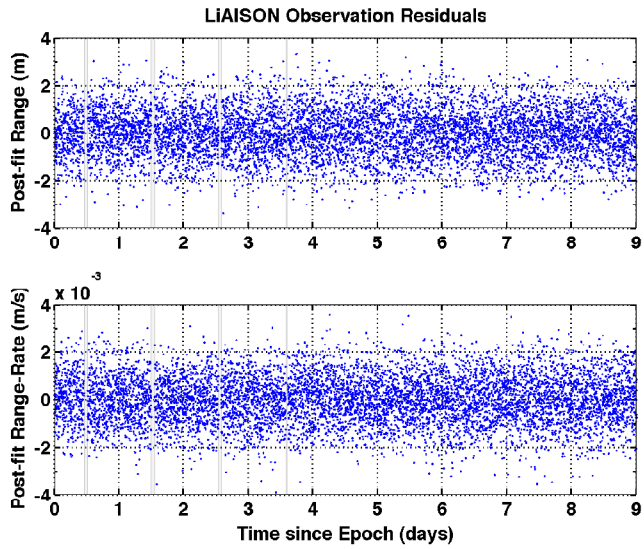

Figure 14. Time evolution of the post-fit residuals. The post-fit RMS for the range is 0.98756 m and for the range-rate is 1.0002 mm/s.

VI. Applications

The LiAISON technology has the potential of providing navigation data to any location that the communication system can reach in the Earth-Moon system. Previous work has demonstrated the capability of LiAISON between lunar assets; this study has explored the potential for LiAISON to span from the lunar libration orbits to geostationary orbit. The lunar libration orbits, such as the LL_1 halo orbit studied here, provide locations where a single navigation satellite can support other satellites anywhere in the Earth-Moon system.

The LiAISON concept permits autonomous navigation, but it is more likely that there will be ground tracking support. As a supplement to ground tracking, LiAISON improves the navigation accuracy and/or dramatically reduces the number of ground tracks required to support a mission. Multiple architectures are viable, including a scenario where a single navigation satellite supports multiple customers by establishing independent two-way links with each, or a scenario where a single navigation satellite supports multiple customers by broadcasting a navigation beacon, much like GPS. Of course in that scenario each satellite requires an accurate clock, though the Deep Space Atomic Clock (DSAC) that is currently being developed at JPL with funding by the NASA OCT is pushing the envelop for the size, mass, and power requirements of space-ready precision clocks. LiAISON may also be a viable technology to add to a spacecraft already aiming for a lunar libration orbit. The relative range and range-rate information may enable low-cost rendezvous operations in lunar libration orbits, low-cost station keeping, and precision landings on the far side of the Moon.

VII. Conclusions

This study demonstrates the viability of obtaining both relative and absolute navigation knowledge using just satellite-to-satellite range and range-rate measurements between a GEO satellite and a satellite in orbit about the Earth-Moon L_1 point. LiAISON has been shown to work in the past for constellations in various orbits near the Moon. This is the first study that demonstrates LiAISON's potential benefits at the Earth as well as near the Moon. The navigation technology has been shown to achieve navigation accuracies consistent with the noise in the observations. In this study, the range observations have been corrupted by 1-meter white noise; the resulting navigation demonstrated that each satellite's position was known to within approximately 1 meter. The scenarios studied are representative of realistic navigation, though many simplifications have been made in order to focus on the core hypothesis: that absolute navigation is possible using relative radiometric tracking data between a GEO satellite and a lunar libration orbiter.

A. Acknowledgements

The authors would like to thank the JPL Center Innovation Fund (CIF) Program, sponsored by the NASA Office of the Chief Technologist (OCT), which has supported this research.

The research presented in this paper has been partially carried out at the Jet Propulsion Laboratory, California Institute of Technology, under a contract with the National Aeronautics and Space Administration.
Copyright 2012 California Institute of Technology. Government sponsorship acknowledged.

References

[1]Hill, K., Lo, M. W., and Born, G. H., "Linked, Autonomous, Interplanetary Satellite Orbit Navigation (LiAISON)," *Proceedings of the AAS/AIAA Astrodynamics Specialist Conference held 7-11 August 2005, South Lake Tahoe, California, Paper AAS 05-399*, edited by B. G. Williams, L. A. D'Amario, K. C. Howell, and F. R. Hoots, Vol. 123 of *Advances in Astronautical Sciences*, AAS/AIAA, Univelt Inc., San Diego, CA, 2006.

[2]Hill, K., Born, G. H., and Lo, M. W., "Linked, Autonomous, Interplanetary Satellite Orbit Navigation (LiAISON) in Lunar Halo Orbits," *Proceedings of the AAS/AIAA Astrodynamics Specialist Conference held 7-11 August 2005, South Lake Tahoe, California, Paper AAS 05-400*, edited by B. G. Williams, L. A. D'Amario, K. C. Howell, and F. R. Hoots, Vol. 123 of *Advances in Astronautical Sciences*, AAS/AIAA, Univelt Inc., San Diego, CA, 2006.

[3]Hill, K., Parker, J. S., Born, G. H., and Demandante, N., "A Lunar L2 Navigation, Communication, and Gravity Mission," *AIAA/AAS Astrodynamics Specialist Conference*, No. AIAA 2006-6662, AIAA/AAS, Keystone, Colorado, August 2006.

[4]Hill, K., Lo, M. W., and Born, G. H., "Liaison Navigation in the Sun-Earth-Moon Four-Body Problem," *Proceedings of the AAS/AIAA 16th Spaceflight Mechanics Meetings held 22-26 January 2006, Tampa, Florida, Paper AAS 06-221*, edited by S. R. Vadali, L. A. Cangahuala, J. P. W. Schumacher, and J. J. Guzman, Vol. 124 of *Advances in Astronautical Sciences*, AAS/AIAA, Univelt Inc., San Diego, CA, 2006.

[5]Hill, K. and Born, G. H., "Autonomous Interplanetary Orbit Determination Using Satellite-to-Satellite Tracking," *AIAA Journal of Guidance, Control, and Dynamics*, Vol. 30, No. 3, May–June 2007.

[6]Hill, K., *Autonomous Navigation in Libration Point Orbits*, Ph.D. thesis, University of Colorado, Boulder, Colorado, 2007.

[7]Villac, B., Chow, C., Lo, M., Hintz, G., and Nazari, Z., "Dynamic Optimization of Multi-Spacecraft Relative Navigation Configurations in the Earth-Moon System," *AAS George H. Born Symposium*, AAS, Boulder, Colorado, 13–14 May 2010.

[8]Hamera, K., Mosher, T., Gefreh, M., Paul, R., Slavkin, L., and Trojan, J., "An Evolvable Lunar Communication and Navigation Constellation Concept," *IEEE Aerospace Conference*, No. IEEE 1491, IEEE, Big Sky, Montana, 28 April–1 May 2008.

[9]Leonard, J. M., McGranaghan, R. M., Fujimoto, K., Born, G. H., Parker, J. S., and Anderson, R. L., "LiAISON-Supplemented Navigation for Geosynchronous and Lunar L1 Orbiters," *Submitted to the AIAA/AAS Astrodynamics Specialist Meeting*, Minneapolis, Minnesota, 13–16 August 2012.

[10]Liu, Y. and Liu, L., "Orbit Determination Using Satellite-to-Satellite Tracking Data," *Chinese Journal of Astronomy and Astrophysics*, Vol. 1, No. 3, 2001, pp. 281–286.

[11]Wallace, S., Sabol, C., and Carter, S., "Optical Sensor Calibration using GPS Reference Orbits," *MIT/Lincoln Lab Space Control Workshop*, Lexington, MA, March 1997.

[12]Sabol, C. A., *A role for Improved Angular Observations in Geosynchronous Orbit Determination*, Ph.D. thesis, University of Colorado, Boulder, Colorado, 1998.

[13]Moreau, M. C., Axelrad, P., Garrison, J. L., and Long, A., "GPS Receiver Architecture and Expected Performance for Autonomous Navigation in High Earth Orbits," *Navigation*, Vol. 47, No. 3, 2000, pp. 191–204.

[14]Tombasco, J., *Orbit Estimation of Geosynchronous Objects via Ground-Based and Space-Based Optical Tracking*, Ph.D. thesis, University of Colorado, Boulder, Colorado, 2011.

[15]Bamford, W., Naasz, B., and Moreau, M. C., "Navigation Performance in High Earth Orbits Using Navigator GPS Receiver," *Proceedings of the 29th Annual AAS Rocky Mountain Guidance & Control Conference held February 4-8, 2006, Breckenridge, Colorado, Paper AAS 06-045*, edited by S. D. Jolly and R. D. Culp, Vol. 125 of *Advances in Astronautical Sciences*, AAS, Univelt Inc., San Diego, CA, 2006.

[16]Broschart, S. B., Chung, M. J., Hatch, S. J., Ma, J. H., Sweetser, T. H., Weinstein-Weiss, S. S., and Angelopoulos, V., "Preliminary Trajectory Design for the ARTEMIS Lunar Mission," *Proceedings of the AAS/AIAA Astrodynamics Specialist Conference held 9-13 August 2009, Pittsburgh, Pennsylvania, Paper AAS 09-382*, edited by A. V. Rao, T. A. Lovell, F. K. Chan, and L. A. Cangahuala, Vol. 134 of *Advances in Astronautical Sciences*, AAS/AIAA, Univelt Inc., San Diego, CA, 2009.

[17]Woodard, M., Folta, D., and Woodfork, D., "ARTEMIS: The First Mission to the Lunar Libration Orbits," *21st International Symposium on Space Flight Dynamics*, Centre National d'Études Spatiales, Toulouse, France, September 28 – October 2, 2009.

[18]Folta, D., Woodard, M., and Cosgrove, D., "Stationkeeping of the First Earth-Moon Libration Orbiters: The ARTEMIS Mission," *Proceedings of the AAS/AIAA Astrodynamics Specialist Conference held 31 July–4 Aug 2011, Girdwood, Alaska, Paper AAS 11-515*, edited by H. Schaub, B. C. Gunter, R. P. Russell, and W. T. Cerven, Vol. 142 of *Advances in Astronautical Sciences*, AAS/AIAA, Univelt Inc., San Diego, CA, 2012.

[19]Woodard, M., Cosgrove, D., Morinelli, P., Marchese, J., Owens, B., and Folta, D., "Orbit Determination of Spacecraft in Earth-Moon L1 and L2 Libration Point Orbits," *Proceedings of the AAS/AIAA Astrodynamics Specialist Conference held July 31 to August 4, 2011, in Girdwood, Alaska, Paper AAS 11-514*, edited by H. Schaub, B. C. Gunter, R. P. Russell, and W. T. Cerven, Vol. 142 of *Advances in Astronautical Sciences*, AAS, Univelt Inc., San Diego, CA, 2012.

[20]Hamilton, T. W. and Melbourne, W. G., "Information Content of a Single Pass of Doppler Data from a Distant Spacecraft," *JPL Space Programs Summary*, Vol. 3, No. 37–39, 1966, pp. 18–23.

[21]Szebehely, V., *Theory of Orbits: The Restricted Problem of Three Bodies*, Academic Press, New York, 1967.

[22]Moulton, F. R., "Periodic Orbits," *Carnegie Institute of Washington Publications*, , No. 161, 1920.

[23]Strömgren, E., "Connaissance actuelle des orbites dans le problème des trios corps," *Copenhagen Observatory Publications*,

, No. 100, 1935, also *Bull. Astr.* Vol. 9, No. 87, 1935.

[24]Broucke, R. A., "Periodic Orbits in the Restricted Three-Body Problem with Earth-Moon Masses," Tech. Rep. 32-1168, Jet Propulsion Laboratory, California Institute of Technology, 1968.

[25]Hénon, M., "Exploration Numérique du Problème des Trois Corps, (I), Masses Egales, Orbites Périodiques," *Ann. Astrophys.*, Vol. 28, No. 3, 1965, pp. 499–511.

[26]Bray, T. A. and Goudas, C. L., "Doubly-Symmetric Orbits about the Collinear Lagrange Points," *The Astronomical Journal*, Vol. 72, No. 2, March 1967.

[27]Farquhar, R. W., *The Control and Use of Libration-Point Satellites*, Ph.D. thesis, Department of Aeronautics and Astronautics, Stanford University, Stanford, CA, 1968.

[28]Breakwell, J. V. and Brown, J. V., "The Halo Family of 3-Dimensional Periodic Orbits in the Earth-Moon Restricted 3-Body Problem," *Celestial Mechanics*, Vol. 20, November 1979, pp. 389–404.

[29]Howell, K. C., "Three-Dimensional, Periodic, 'Halo' Orbits," *Celes. Mech.*, Vol. 32, No. 1, 1984, pp. 53–71.

[30]Richardson, D. L., "Analytical Construction of Periodic Orbits about the Collinear Points," *Celestial Mechanics*, Vol. 22, 1980, pp. 241–253.

[31]Farquhar, R. W. and Kamel, A. A., "Quasi-Periodic Orbits about the Translunar Libration Point," *Celestial Mechanics*, Vol. 7, No. 4, June 1973, pp. 458–473.

[32]Gómez, G., Masdemont, J., and Simó, C., "Quasihalo Orbits Associated with Libration Points," *The Journal of the Astronautical Sciences*, Vol. 46, No. 2, 1998, pp. 135–176.

[33]Farquhar, R. W., "Station-Keeping in the Vicinity of Collinear Libration Points with an Application to a Lunar Communications Problem," *Space Flight Mechanics*, Vol. 11 of *Science and Technology Series*, American Astronautical Society, New York, 1966, pp. 519–535.

[34]Farquhar, R. W., "Lunar Communications with Libration-Point Satellites," *Journal of Spacecraft and Rockets*, Vol. 4, No. 10, 1967, pp. 1383–1384.

[35]Clarke, A. C., *Interplanetary Flight*, Temple Press Books Ltd., London, 1950.

[36]Parker, J. S., *Low-Energy Ballistic Lunar Transfers*, Ph.D. thesis, University of Colorado, Boulder, Colorado, 2007.

[37]Standish, E. M., "JPL Planetary and Lunar Ephemerides, DE405/LE405," Tech. Rep. IOM 312.F–98–048, Jet Propulsion Laboratory, California Institute of Technology, August 1998.

[38]Parker, J. S., "Monthly Variations of Low-Energy Ballistic Transfers to Lunar Halo Orbits," *AIAA/AAS Astrodynamics Specialist Conference*, No. AIAA 2010-7963, AIAA/AAS, Toronto, Ontario, Canada, August 2–5, 2010.

[39]Richardson, D. L. and Cary, N. D., "A Uniformly Valid Solution for Motion of the Interior Libration Point for the Perturbed Elliptic-Restricted Problem," *Proceedings of the AAS/AIAA Astrodynamics Specialist Conference held 28-30 July 1975, Nassau, Bahamas, Paper AAS 75-021*, edited by W. F. Powers, H. E. Rauch, B. D. Tapley, and C. E. Velez, Vol. 33 of *Advances in Astronautical Sciences*, AAS/AIAA, Univelt Inc., San Diego, CA, 1976.

[40]Wilson, R., "Derivation of Differential Correctors Used in GENESIS Mission Design," Tech. Rep. JPL IOM 312.I-03-002, Jet Propulsion Laboratory, California Institute of Technology, 2003.

[41]Pernicka, H. J., *The Numerical Determination of Lissajous Orbits in the Circular Restricted Three-Body Problem*, Master's thesis, Purdue University, West Lafayette, Indiana, December 1986.

[42]Parker, J. S. and Born, G. H., "Direct Lunar Halo Orbit Transfers," *Proceedings of the 17th AAS/AIAA Spaceflight Mechanics Meetings held 28 Jan–1 Feb 2007, Sedona, Arizona, Paper AAS 07-229*, edited by M. R. Akella, J. W. Gearhart, R. H. Bishop, and A. J. Treder, Vol. 127 of *Advances in Astronautical Sciences*, AAS/AIAA, Univelt Inc., San Diego, CA, 2007.

[43]Parker, J. S. and Born, G. H., "Direct Lunar Halo Orbit Transfers," *Journal of the Astronautical Sciences*, Vol. 56, No. 4, Oct–Dec 2008.

[44]Tapley, B. D., Schutz, B. E., and Born, G. H., *Statistical Orbit Determination*, Elsevier Academic Press, Burlington, MA, 2004.

[45]Prince, P. J. and Dormand, J. R., "High Order Embedded Runge-Kutta Formulae," *Journal of Computational and Applied Mathematics*, Vol. 7, 1981, pp. 67–75.

[46]Cramér, H., *Mathematical Methods of Statistics*, Princeton University Press, Princeton, New Jersey, 1946.

[47]Rao, C. R., "Information and the Accuracy Attainable in the Estimation of Statistical Parameters," *Bulletin of the Calcutta Mathematical Society*, Vol. 37, 1945, pp. 81–89.

[48]Rao, C. R., *Selected Papers of C. R. Rao*, Wiley, New York, 1994.

[49]Taylor, J. H., "The Cramér-Rao Estimation Error Lower Bound Computation for Deterministic Nonlinear Systems," *IEEE Transactions on Automatic Control*, Vol. AC-24, No. 2, 1979, pp. 343–344.

[50]Ma, C., Arias, E. F., Eubanks, T. M., Fey, A. L., Gontier, A. M., Jacobs, C. S., Sovers, O. J., Archinal, B. A., and Charlot, P., "The International Celestial Reference Frame as Realized by Very Long Baseline Interferometry," *The Astronomical Journal*, Vol. 116, July 1998, pp. 516–546.